Ann. Phys. (Berlin) 524, No. 3–4, 212–226 (2012) / DOI 10.1002/andp.201100269

annalen der physik

Original Paper

Spin excitations in Co_2NiGa under pressure from a theoretical approach

Emilia Olivos[1,*], *Alonso L. Miranda*[1], *Navdeep Singh*[2], *Raymundo Arróyave*[2,3], *and Aldo H. Romero*[1]

Received 14 October 2011, revised 20 December 2011, accepted 21 December 2011
Published online 6 February 2012

Dedicated to Ulrich Eckern on the occasion of his 60th birthday.

The Heisenberg exchange parameters for the Heusler compound Co_2NiGa with $L2_1$ structure were calculated using the Korringa–Kohn–Rostoker method and by employing the magnetic-force theorem to obtain the total energy changes associated with the local rotation of magnetization direction. The crystal structure was subjected to pressure and the corresponding dependence of the magnetic exchange couplings were determined. Curie temperatures obtained by applying mean field theory (MFT) reveals a slightly nonlinear decrease with pressure and it is related to the changes of the magnetic moment and the electronic density of states. Further investigation of the pressure dependence of the Curie temperature and magnetization suggests that this particular compound is a weak itinerant ferromagnet. Analysis of the magnetic properties of the Co_2NiGa compound using Monte Carlo simulations reveals a significant effect of pressure on the magnetization and magnetic susceptibility of the structure. The spin dynamics was modeled by applying the Landau-Lifshitz-Ginzburg equation to a Heisenberg Hamiltonian. The magnon spectra along the [100] direction is obtained through the Fourier transform of the dynamic correlation function for the predefined set of exchange parameters and pressure. We find a large dependence of the magnon dispersion relation with pressure and in particular of the magnetic excitations gap.

1 Introduction

Heusler alloys are magnetic multi-component intermetallic alloys with XYZ (half Heusler) or X_2YZ (full Heusler) stoichiometries. These alloys are based on the face-centered cubic structure with half Heusler alloys having the $C1_b$ structure and full Heusler alloys having the $L2_1$ structure, although in some cases the latter can also exist – as a result of a disorder transition – in the B2 structure. These alloys can be metallic or even semiconducting, although most of them are half-metallic. The half-metallicity relates to the fact that many of these alloys have a significant population of uncompensated electrons between the minority and majority spin states at the Fermi energy. Due to these localized or itinerant electrons, ground states can present many different physical properties with several complex forms such as ferromagnetism or antiferromagnetism. Owing to their complex magnetic behavior, these alloys possess specific properties that make them immensely interesting in the field of actuation, sensing and spintronics, among other applications [1–4].

In addition, some Heusler alloys exhibit a structural phase transition. This transition sometimes, correlates with changes in the magnetic state [5] that can be controlled by the application of a magnetic field and/or temperature (magnetic shape memory effect). In ferromagnetic shape memory (Heusler) alloys (FSMAs) external magnetic fields and/or stress/temperature can trigger a thermoelastic structural – martensitic – transition from the high temperature austenite phase, which usually has cubic symmetry, to the low temperature martensitic phase, always of lower symmetry than the austenite phase and often of tetragonal symmetry in Heusler FSMAs. In some FSMAs, large magnetic entropy changes associated with the martensitic transformation can result

* Corresponding author E-mail: eolivos@qro.cinvestav.mx
[1] CINVESTAV, Departamento de Materiales, Unidad Querétaro, Querétaro, 76230, Mexico
[2] Department of Mechanical Engineering, Texas A & M University, College Station, Texas, USA
[3] Materials Science and Engineering Program, Texas A & M University, College Station, Texas, USA

in significant inverse magneto-caloric effects and a large dependence of the Curie temperature with respect to the applied pressure [6]. This property is of great importance for applications such as cooling and heating devices, actuators and sensors [7, 8].

The family of Co_2 Heusler ferromagnets (HF) is one of the most interesting classes of materials for spintronic applications [9]. This is mainly due to the ability of these materials to make good ferromagnetic contacts which act as polarizers for the transported spins. These materials possess good spin polarization at the Fermi level, an important property for spin transport. It is of great interest to explore the possibility of full HF with stoichiometry X_2YZ having this electronic property.

Many of the alloys discussed above also possess high Curie temperature, which makes them of relevance in new magnetic devices. To integrate Heusler alloys to the main-stream devices, there is an on going need to understand the origin of the reduction in the idealized 100% spin polarization at finite temperature or stress. It is, therefore, of great importance to see the effect of thermal excitations (phonons, magnons, etc), due to temperature or pressure, on the different properties of these alloys. On the other hand, due to the half-metallicity of some of these systems, the electron population and hence the electronic properties of these alloys can be modified by the application of external fields. Also, processes involving magnons (electron-magnons, magnon-magnon scattering, phonon-magnons and thermal excitation of magnons) are believed to strongly contribute to the decay of the spin polarization with temperature.

Special technological attention has been paid to separate class of functional materials based on $Co_2Ni(Ga,Al)$ alloys, as these can be reversibly controlled both in shape and size by the application of mechanical stresses [10] or magnetic fields [11]. The martensitic transition is accompanied by a one-way or two-way shape memory effect and superelasticity making them very promising for magnetically controlled devices like actuators, sensors as well as active structures. There are several literature reviews and research papers on the electronic and structural characterization of this material [10–12], but only few take into account the magnon contribution. In particular, the authors did not find any work considering the magnon contribution to properties of Co_2NiGa alloy, including the effects of pressure. As will be seen below, understanding the effects of pressure on the properties of this alloy system is not only scientifically relevant but also it allows us to correlate changes of the magnetic moment as function of pressure to the volume magnetostriction through a Maxwell relation [13].

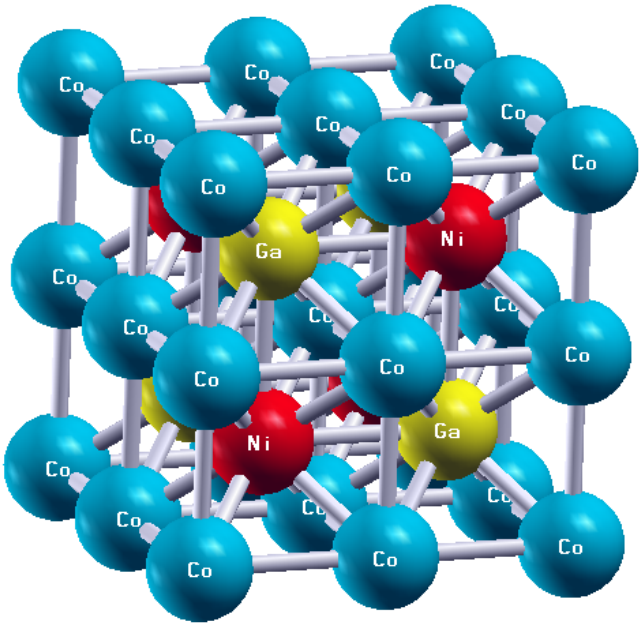

Figure 1 (online color at: www.ann-phys.org) Cubic crystal structure of Co_2NiGa with space group no. 225, Fm3m. Every atom in the unit cell occupies a face centered cubic (FCC) sub-lattice.

The focus of this paper is to reveal some of the magnetic properties of Co_2NiGa dependence with respect to pressure and to correlate them with magnetostriction and temperature. We try to embody different methodologies into a series of calculations that study the magnetic changes of a $L2_1$ structure alloy and to develop a coherent picture of the magnetic changes as function of the electronic and thermal properties.

This paper is divided as follows: Sect. 2 gives a discussion of some theoretical tools used in our calculations, proper references are included. Section 3 presents the computational details used for the data we are developing in Sect. 4. In particular, Sect. 4 describes the magnetic properties of this system as function of pressure as well as the magnon spectra along the [100] direction. Section 5 finishes up this work by describing the conclusions and the ongoing efforts to improve the understanding of the magnetic changes along structural phase transitions in Heusler alloys.

2 Formalism

The structural properties were obtained from a density functional theory (DFT) calculation as implemented in

the software VASP [14, 15] and the magnetic exchange coupling constants for Co_2NiGa alloy were obtained using the SPRKKR package [16–18]. The SPRKKR method is based on a Green's function approach. These functions are determined by treating the solid as a multi stray system. The perturbing potentials for each atom are assumed to be spherically symmetric without overlapping (atomic sphere approach, ASA). The equations describing the electronic properties are based on the solution of the Dirac equation with relativistic contributions, which are important for magnetic systems.

The magnetic exchange interaction constants J_{ij} have been determined by mapping the problem onto a classical Heisenberg model:

$$\mathbf{H} = -\frac{1}{2}\sum_{i\neq j} J_{ij}\mathbf{m}_i \cdot \mathbf{m}_j \tag{1}$$

where i and j are atomic indices, J_{ij} represents the magnetic exchange coupling and $\mathbf{m}$ are the unitary local magnetic moments. J_{ij} are calculated using *ab initio* calculation based on the KKR method. This method employs the magnetic-force theorem to calculate the total energy changes associated with the local rotation of magnetization directions using the formulation proposed by Lichtenstein [19]:

$$J_{ij} = \frac{1}{4\pi}\int^{\epsilon_F} \mathrm{Im}\,\mathrm{Tr}_L\{\Delta_i \hat{T}^{ij}_{\uparrow}\hat{T}^{ij}_{\downarrow}\}\,\mathrm{d}\epsilon. \tag{2}$$

where Δ_i is the difference in the inverse single-site scattering matrices for spin up and spin down electrons. Tr_L denotes the trace over the product of the scattering matrices with respect to the orbital L and $\hat{T}$ is the scattering path operator. Using the magnetic exchange parameters, within the mean-field approximation (MFA), the Curie temperature of the system is obtained as [20, 21]:

$$\frac{3}{2}k_B T_c^{MFA} = \sum_{\nu} J^{\mu\nu}_{m,0}\langle \mathrm{e}^{\nu}\rangle \tag{3}$$

and

$$J^{\mu\nu}_{m,0} = \sum_{R\neq 0 \text{ when } \mu=\nu} J^{\mu\nu}_{m,0R} \tag{4}$$

In equation (4), the magnetic exchange parameter $J^{\mu\nu}_{m,0}$ is obtained by summing all exchange parameters involving the sublattices μ and ν, including all equivalent sublattices ν translated by lattice vector R, *except when* $\mu = \nu$ *in the first unit cell* ($R = 0$).

Rewriting these equations, we have the following eigenvalue problem:

$$(\Theta - TI)E = 0, \qquad \frac{3}{2}k_B\Theta_{\mu\nu} = J^{\mu\nu}_{m,0} \tag{5}$$

where $J^{\mu\nu}_{m,0}$ is the magnetic exchange parameter between sublattices μ and ν, k_B is the Boltzmann's constant, I is the identity matrix, $E^{\nu} = \langle \mathrm{e}^{\nu}\rangle$, where $\langle \mathrm{e}^{\nu}\rangle$ is the average z component of the unit vector, $\langle \mathrm{e}^{\nu}_R\rangle$. The Curie temperature of the system corresponds to the largest eigenvalue of Θ [20, 21].

From the Heisenberg Hamiltonian, the effective interaction field experienced by each atomic moment $\mathbf{B}_i$ is calculated as,

$$\mathbf{B}_i = -\frac{\partial H}{\partial \mathbf{m}_i}. \tag{6}$$

This equation gives the average field felt by the magnetic moments due to the presence of the others. By including different ranges of the magnetic exchange coupling, in principle, this Hamiltonian can capture the magnetic structure in great detail. In fact, the results are very close to that obtained in an electronic structure code, unless some specific electronic transfer could occur, which is not captured by the assumption of constant magnetic exchange couplings.

The Heisenberg model in Eq. 1 can be Fourier-transformed by using the periodicity of the lattice, such that

$$\mathbf{m}(\mathbf{q}) = \frac{1}{N}\sum_n \mathbf{m}_n \mathrm{e}^{-i\mathbf{q}\cdot\mathbf{R}_n} \tag{7}$$

$$J(\mathbf{q}) = \sum_n J_{0n}\mathrm{e}^{-i\mathbf{q}\cdot\mathbf{R}_n} \tag{8}$$

where $\mathbf{q}$ corresponds to a reciprocal lattice vector. Thus we obtain

$$H = -N\sum_{\mathbf{q}} J(\mathbf{q})\mathbf{m}(\mathbf{q})\cdot\mathbf{m}(-\mathbf{q}) \tag{9}$$

where the magnitude of the local magnetic moment needs to be guaranteed. This condition is fulfilled by a periodic solution with given perpendicular unitary vectors, which describe a spiral spin density wave (SSDW). The propagating excitation maximizes the magnetic exchange coupling along a specific $\mathbf{q}$. In general, at low temperatures, these collective excitations can be excited in a magnetic crystal, with the main feature being a quadratic dispersion close to the Γ point.

Usually, the dependence of magnetic excitations are calculated from first principles, by using the "frozen-magnon" approach. This approach relies on rigid spiral rotations of the magnetic moments and their effect on the energy changes. This approach has two main drawbacks. First, it is computationally very expensive and depending on the $\mathbf{q}$, a large supercell is required. Second, it relies on the harmonic approximation of the energy with respect to the rotation of the magnetic moment.

Another approach is to consider the autocorrelation function of the magnetic moments of a dynamically-correct system. For such purpose, a dynamical set of equations for the magnetic moments are considered and the magnetic configuration is autocorrelated for a large number of iterations. The dynamical structure factor can be obtained from the time-dependent Fourier transform of the average magnetic moment-magnetic moment correlation function,

$$C(\mathbf{r}', t') = \langle \mathbf{m}(\mathbf{r}, t) \cdot \mathbf{m}(\mathbf{r} + \mathbf{r}', t + t') \rangle, \tag{10}$$

This quantity is a good measure of the structure and equilibration of the spin system. In order to evaluate the spin wave excitations, one may calculate S($\mathbf{q}$,ω) by performing a space and time Fourier transform of the spin-spin correlation, also called dynamic structure factor,

$$S(\mathbf{q}, \omega) = \int d\mathbf{r} e^{-i\mathbf{q}\cdot\mathbf{r}} \int dt e^{i\omega t} C(\mathbf{r}, t) \tag{11}$$

Now, if the rotation of the magnetic moments have an oscillatory behavior, the magnetic moment direction will be correlated and it will come as a feature in the dynamical structure factor. Sharp peaks in this quantity indicates the existence of well-defined excitations, that correspond in turn to the magnons.

The temporal evolution of the atomic spins at finite temperature is modeled using Langevin dynamics, through the phenomenological coupled stochastic differential equations discussed by Landau-Lifshitz-Gilbert (LLG) [22, 23]. This description is valid as long as the wavelength is large compared to the lattice parameter. Within this approximation, a fixed length magnetization vector precesses in response to an applied magnetic field, which tries to rotate it.

$$\frac{d\mathbf{m}_i}{dt} = -\gamma \mathbf{m}_i \times [\mathbf{B}_i + \mathbf{b}_i(t)] - \gamma \frac{\alpha}{m} \mathbf{m}_i \times (\mathbf{m}_i \times [\mathbf{B}_i + \mathbf{b}_i(t)]). \tag{12}$$

In this expression, γ is the the electron gyromagnetic ratio, and $\mathbf{b}_i$ is a stochastic magnetic field with a Gaussian distribution, the magnitude of which is related to the temperature and the phenomenological damping parameter α, which eventually brings the system to thermal equilibrium. This approach has been recently implemented in the software atomistic spin dynamics (ASD) [24, 25]. On the right-hand side of equation Eq. (12) the first term corresponds to the torque driving precessional magnetization motion around the effective field, and the second term expresses the friction torque. Studies have revealed that Gilbert magnetic damping is an intrinsic property in ferromagnetic metals, as well as magnetic moment or resistivity if one excludes any other extrinsic influences, e.g. magnetic inhomogeneities and two-magnon scattering [26, 27]. Nowadays, magnetic damping is predicted from theoretical expressions and combined with first-principle band structure calculation [28].

3 Computational details

Our investigations have been carried out in the framework of density functional theory using the plane wave code VASP [14]. The electron ionic core interaction has been accounted for by applying the PAW method [15] and the exchange correlation energy has been expressed using the GGA exchange-correlation potential of Perdew, Burke, and Ernzerhoff [29]. All calculations have been performed under the Local Spin Density Approximation to account for the spin density distribution. For the Brillouin-zone sampling, we use a $13 \times 13 \times 13$ Monkhorst-Pack k-point mesh. The energy cut-off was chosen to be 470 eV. With these fixed variables a very good energy convergence has been observed. After the ground state structure has been obtained, a sweep over a range of pressure values was performed and the compressibility curve was adjusted accordingly. The equation of state defining the relationship between pressure and the volume has been used in the proceeding calculations, as well as the optimized VASP structural parameters.

The unit cell from the previous calculations have been used to perform calculations with spin polarized relativistic Korringa-Kohn-Rostoker (SPRKKR) [16, 17] software to fix unit cell. Atomic sphere approximation (ASA) geometry is considered for the charge density and potential. This package allows the calculation of electronic structure of arbitrary three-dimensional periodic systems. The exchange correlations used in this step corresponds to the same functional used in the VASP calculations. The calculated electronic density of states using both the codes agree well with each other and reveal the identical physical picture of the system. We have also made sure that the parameters used in the SPRKKR calculation corresponds closely to the ones used in the VASP calculation e.g. same exchange correlation, a large number of K points and the spin polarization. In the SPRKKR calculations, the angular momentum expansion was truncated after $l_{\max} = 3$ component. 500 k-points have been chosen using the special points method and accordingly, for each pressure, the Wigner-Seitz radii (in Å) has been chosen. The effect of pressure has been taken into account by changing the volume according to the fit-

ted equation of state and *using the initial cell parameter optimized from the VASP code*. The exchange parameters, $\mathbf{J}_{ij}$, for ground state structures and structures under pressure, have been calculated using the method outlined in the previous section.

The calculated magnetic moments and the exchange couplings have been used to determine the spin changes as function of time using the spin dynamics code (ASD). The time evolution of the spin dynamics has been explicitly simulated by treating the equation of motion for the atomic magnetic moments. The central entity of the technique are the microscopic equations of motion for the atomic moments, $\mathbf{m}_i$ Eq. (12), in an effective field $\mathbf{B}_i$ Eq. (6). The isotropic exchange interactions have been treated by introducing the classical Hamiltonian Eq. (1). In order to study the $L2_1$ structure Co_2NiGa along the [100] direction, a supercell of $150 \times 10 \times 10$ cell with periodic boundary conditions, encompassing 60000 atomic spins and four different pressure values (P = 0, 6, 12, 18 GPa). The 150 cells guarantees to sample 150 $\mathbf{q}$ along the [100]. We have considered 5 unit cells in other directions to be able to describe the correct decay of the magnetic exchange couplings with neighbors along those directions. In the initial step of the simulation, the spin systems have been equilibrated with a heat bath at $T = 100$ K, with damping term $\alpha = 0.01$ for pressures smaller than 6.0 GPa and $\alpha = 0.001$ for larger pressures. The dynamical structure factor $S(\mathbf{q}, \omega)$ has been obtained from calculations performed with a time interval of 10.0 ps and time step of 0.5 fs.

The choice of the damping parameter has been based on the values reported for similar Heusler alloys [30]. The dependence of the damping parameter with increase in pressure is not exactly known but it has been found that there is a strong relation between the electronic DOS with the damping value. The correlation between damping parameter and density of states is given through the expression: $\alpha \propto \xi^2 D(E_F)$ [31], where ξ is the spin-orbit coupling parameter for the d-band and $D(E_F)$ is the total density of states in the Fermi energy, E_F [32]. The correlation between α and $D(E_F)$ has been never investigated experimentally but using our calculated DOS, we can modify the damping value accordingly. Several studies have suggested that the Co_2YZ full-Heusler alloy can exhibit a low damping constant because these alloys show soft magnetic properties, probably owing to low orbital magnetic moment [32–34].

Other than describing the spin dynamics, we have also extended this study to calculate the effect of magnetization with change in temperature and pressure. Such calculation can be realized by using Monte Carlo simulations. In these simulations, the Hamiltonian describing the energy of the system is given by the modified Pott's model [35–37]

$$H = \sum_i J_{ij}(2\delta_{S_i S_j} - 1) \tag{13}$$

where J_{ij} is the magnetic exchange parameter between an atom i and its neighbor j, S_i is the spin state of an atom i. Three spin states for Co atoms and two spin states for Ni atom has been considered in these simulations. Since Ga atom is non-magnetic, all the interactions with the Ga atoms have been neglected. The simulation domain consists of a total of 8192 atoms, with 4096 Co atoms, 2048 atoms of Ni and Ga each. The system is equilibrated for 30,000 Monte Carlo steps (MCS) and then simulation is continued for another 30,000 MCS for data collection. The details of the Monte Carlo technique can be found here [37]. At any given temperature, the magnetization and magnetic susceptibility of the system is given by

$$m = \frac{1}{\sum_i^n N_i}\left(\sum_i^n \frac{q_i N_{\max}^i - N_i}{q_i - 1}\right) \tag{14}$$

$$\chi_m = \frac{1}{k_B T^2}[\langle m^2\rangle - \langle m\rangle^2] \tag{15}$$

where N_i is the total number of magnetic atoms of type i, $N_{\max}^i$ is the total number of identical magnetic states of i atom, T temperature of the system and k_B is the Boltzmann's constant.

4 Results

The Co_2NiGa has a cubic crystal structure $L2_1$ with four interpenetrating face-centered cubic sub-lattices with Wyckoff positions defined perfectly by symmetry as (0,0,0) (1/2,1/2,1/2), (1/4,1/4,1/4) and (3/4,3/4,3/4). The crystal structure is illustrated in Fig. 1. The equilibrium cell parameter has been reported in Table 1, which agrees well with the values previously reported [12]. The bulk modulus has been calculated to be 180.2 GPa, which is in good agreement with previous results [12] and also in close agreement with similar Heusler allows such as Ni_2MnGa 156 GPa [38], Ni_2CoGa 194.5 GPa a [39], Fe_2NiGa 146 GPa [40]. Table 1 also reports the next nearest neighbor distances between different atoms in the optimized unit cell. The pressure dependence reveals a non linear decrease in the lattice parameter.

The structural dependence on pressure is characterized by the compressibility factor, which has been found to be $a = 5.457 \times 10^{-3}$ GPa^{-1}, where the relation between

Table 1 Structural and electronic parameters of Co_2NiGa. P corresponds to pressure, a to the equilibrium lattice parameter, T_c to the Curie temperature derived by two different methods: mean field theory (MFT) and Monte Carlo simulations (MCS).

P (GPa)	a (Å)	Distance (Å)			Polarization	T_c (K) (MFT)	T_c (K) (MCS)
		Co–Co	Co–Ni	Ni–Ni			
0.0	5.693	2.847	2.449	4.026	−0.529	395	405
6.0	5.634	2.817	2.423	3.984	−0.533	342	340
12.0	5.583	2.791	2.401	3.947	−0.493	319	310
18.0	5.539	2.769	2.382	3.916	−0.568	272	265

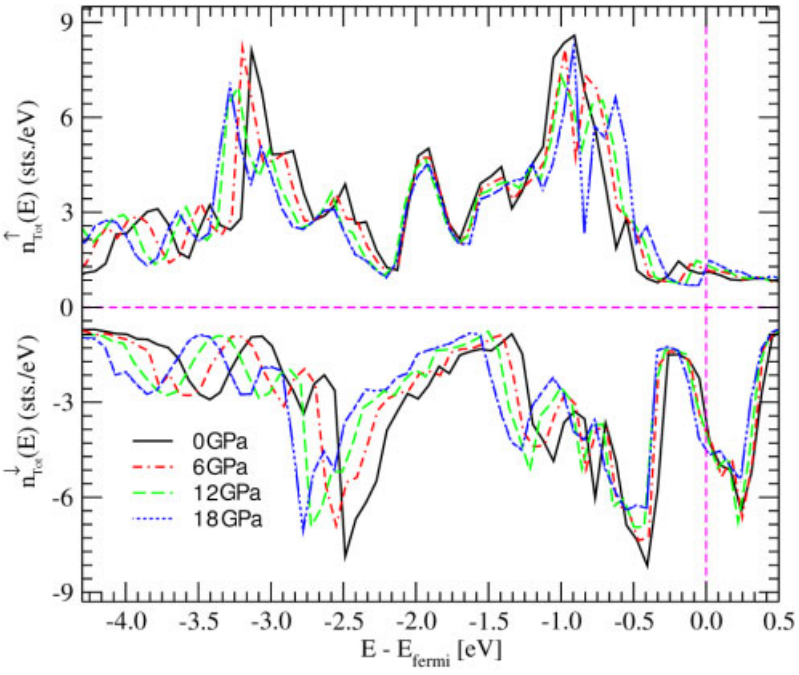

Figure 2 (online color at: www.ann-phys.org) Total electronic density of states of Co_2NiGa for different applied pressures. Energy is reported with respect to the Fermi energy.

the lattice parameter and the applied pressure is given by the following expression:

$$\frac{V - V_0}{V_0} = -aP + bP^2 \tag{16}$$

where V_0 is the volume of the unit cell at ambient pressure and a is the compressibility factor. The compressibility factor obtained in our calculations is of the same order of magnitude as reported for Ni_2MnGa (8.64×10^{-3} GPa^{-1}) measured using experimental techniques [41]. As pressure increases, the atomic distances decreases, as shown in Table 1. This decrease of interatomic distances increases the atomic density overlap and decreases the magnetic moment and the Curie temperature of the system, as will be seen below.

In relation to the electronic properties, the electronic density of states and the contributions from the different atomic elements in the Co_2NiGa alloy is reported in Fig. 2. The atoms which contribute the most to the electronic density of states at the Fermi energy are Ni and Co, with cobalt being the dominant one. As expected, the electronic DOS at the Fermi level is dominated by d-states. Our analysis suggests strong hybridization between the d-states of Co and Ni close to the Fermi level, as shown in an earlier publication by some of the present authors [12].

The polarization increases possibly due to the difference in the hopping electronic rate between different electron channels. The hopping is estimated by integrating the d-character over the occupied bands per channel for Co. Our results go from 4.37 (3.38) e^- at 0 GPa, 4.33 (3.41) e^- at 6 GPa, 4.31 (3.41) e^- at 12 GPa to 4.25 (3.48) e^- at 18 GPa for the majority (minority) spin channel. At low pressures both channels change slowly, while after

Table 2 Atomic magnetic moments and exchange magnetic couplings J_{ij} for Co_2NiGa alloys as a function of pressure. Subindex J_1, J_2, J_3 correspond to the exchange couplings for first, second, third nearest neighbors pairs.

				J_{ij} (meV)								
P	m^{Co}	m^{Ni}	m^{Ga}	Co–Co			Co–Ni			Ni–Ni		
(GPa)	(μ_B)	(μ_B)	(μ_B)	J_1	J_2	J_3	J_1	J_2	J_3	J_1	J_2	J_3
0.0	0.935	0.474	-0.067	3.91	0.75	-1.22, 2.12	4.19	0.19	0.08	-0.06	0.11	0.03
6.0	0.873	0.465	-0.062	3.26	0.69	-1.38, 2.05	3.63	0.18	0.05	-0.08	0.12	0.03
12.0	0.849	0.458	-0.059	3.12	0.70	-1.28, 1.82	3.43	0.18	0.04	-0.07	0.12	0.03
18.0	0.831	0.454	-0.055	2.28	0.86	-0.79, 1.06	2.90	0.17	0.01	-0.07	0.12	0.04

12 GPa the change is much larger. This can be correlated with the changes in the magnetic moment for Cobalt and the change on the total polarization. The change in this integral for the case of Ni is much smaller. From close inspection of the ground state results, there is a large difference between the majority and the minority states at the Fermi level, giving rise to a significant polarization. The spin polarization is defined as $(N_i - N_d)/(N_i + N_d)$, where N_i (N_d) is the spin population of the majority (minority) spin at the Fermi energy and it is reported in Table 1. In case of Co_2NiGa, the polarization is negative, which is typical for cobalt and nickel based alloys due to their small density of states at the Fermi level [42]. As pressure increases, the polarization becomes more negative, from −0.53 at 0 GPa up to −0.57 at 18 GPa. Overall, as pressure increases, the overlap between neighbor atoms is also increased, there is a charge transferred from the d-orbitals, which become less localized and is responsible for the change in the magnetization. At the same same time, the charge transferred is not uniform between the two channels and the polarization is increased. From Table 1 it can be seen that the trend of increased polarization at larger pressures is broken at 12 GPa, where the polarization decreases again, only to become larger at higher pressures.

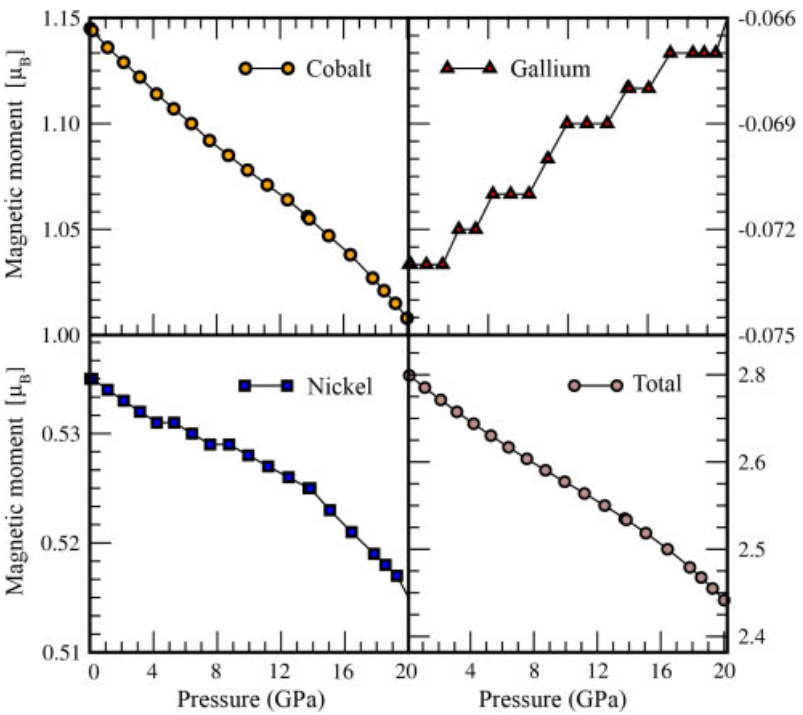

Figure 3 (online color at: www.ann-phys.org) Magnetic moment dependence as function of pressure for Co_2GaNi for every one of the atomic components and the total magnetization in the primitive cell.

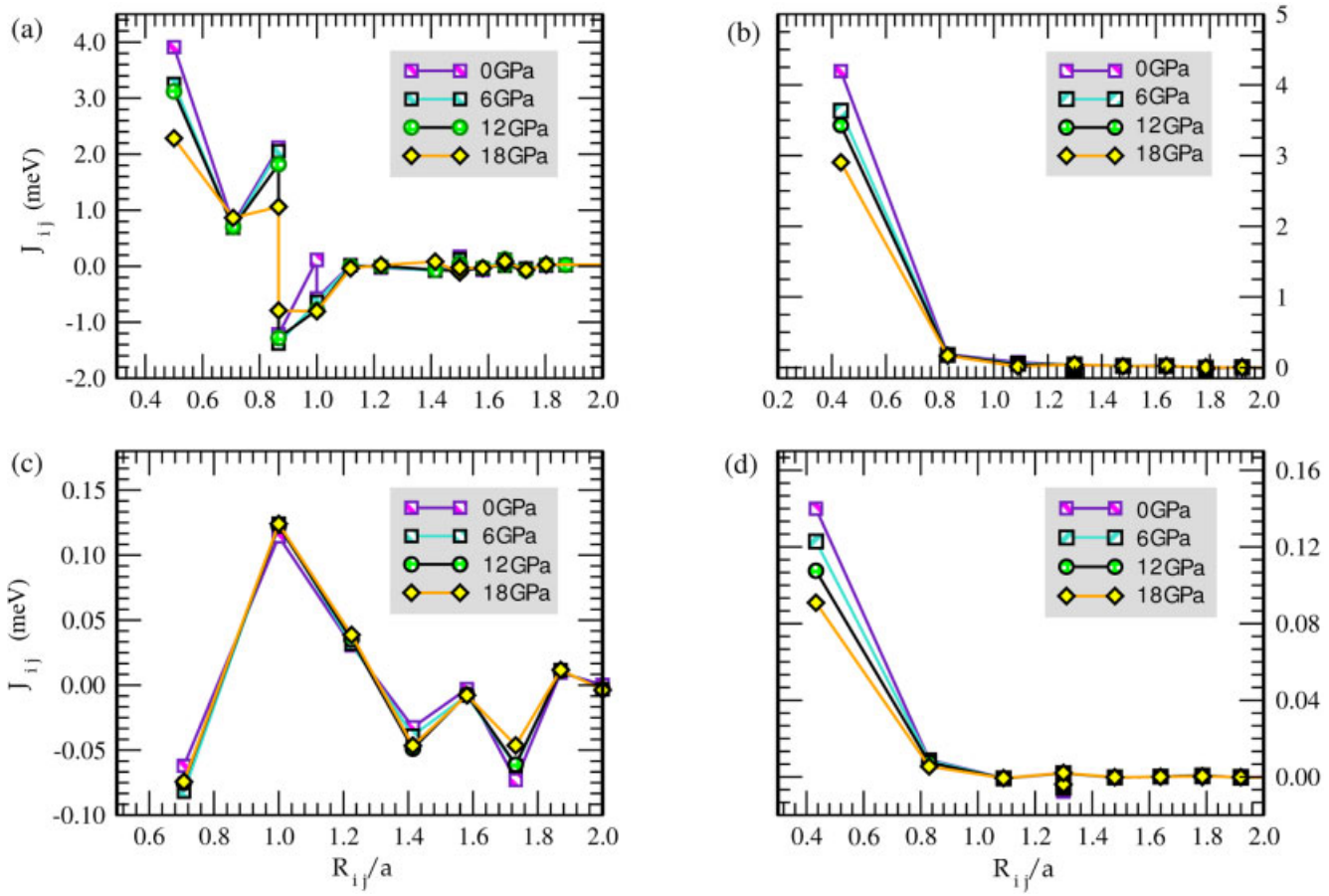

Figure 4 (online color at: www.ann-phys.org) Magnetic exchange couplings of Co_2NiGa as function of pressure. (a) Co–Co (b) Co–Ni (c) Ni–Ni (d) Co–Ga.

We were unable to define a simple functional form to describe the dependence as it was done for the case of temperature [43].

A better insight into the inflections seen in the pressure dependence of polarization (as well as other magnetic properties, as will be seen below) can be obtained by examining the evolution of the majority channel of the total electronic DOS (Fig. 2) as a function of pressure. According to the calculations, from 0 GPa up to about 12 GPa the slope of the density of states $(dn(E)/dE)$ at the Fermi level E_F is negative and the majority electronic density at E_F increases as pressure increases. On the other hand, when the pressure goes past 12 GPa, the slope of the electronic DOS is negative and the prominent peak of the majority channel close to E_F is further displaced to higher energies. As mentioned above, the greatest contributor to electronic states at the Fermi level is the d-band of Co atoms. It thus seems that the qualitative changes in the majority channel of Co (consisting mostly of d electrons) is mostly responsible for the rather significant changes in polarization in the vicinity of 12 GPa. As will be seen below, similar inflections can be observed in other magnetic properties.

The static magnetic properties have been characterized by means of two different observables, the magnetic moment shown in Fig. 3 and magnetic exchange couplings in Fig. 4. The magnetic moment of Co and Ni (1.14 μ_B and 0.535 μ_B, respectively) have been found to be small compared with other transition metals but similar to the values reported in the literature for other Ni and Co based Heusler alloys e.g. in Ni_2CoGa, the magnetic moments are Ni 0.14 μ_B and Co 1.58 μ_B [44], in Co_2VGa the local magnetic moment for Co is 1.05 μ_B [45]. These results suggest that due to the Ni–Co hybridization, the electronic charge is redistributed and the electrons become more metallic and less localized. It has been recognized that for half metallic systems, the total spin magnetic moment scales as the number of valence electrons and follows the Slater-Pauling behavior, $M = Z - 24$, where Z is the valence number of electrons and M is the total magnetic moment of the unit cell [46]. For Co_2NiGa alloy, Slater-Pauling equation gives $M = 7\,\mu_B$ but this value is very large compared to the calculated magnetic

moment of 2.75 μ_B using ab-initio calculations. This discrepancy is due to the Ni–Co hybridization, which decreases the number of available localized electrons thus decreasing the real magnetic moment. A close inspection of the electronic DOS shows that this system is not really half metallic, although the population in the majority channel at the Fermi level is rather small compared to that of the minority states. It is interesting to note that this behavior has been reported for other nickel based Heusler alloys [46].

The behavior of the magnetization as function of pressure is shown in Fig. 3. As pressure increases, the interatomic distance decreases (Table 1). In general, the magnetic moment decreases with an increase in pressure due to an increase of the atomic overlap, when atoms become closer to each other. The calculated magnitude of the magnetization has been reported in Table 2, which shows a decay of the magnetic moment of cobalt by almost 10% (see Table 1). In case of nickel, the decrease is less than 5% and negligibly small in case of gallium. Overall, the magnetization within the unit cell decreases almost by 12.5% with change in pressure of 18 GPa. This change is mostly the result of electron delocalization in cobalt as it is the greatest contributor to the electronic DOS at the Fermi level. From a macroscopic point of view, this decrease in magnetization with pressure is also consistent with positive isotropic magnetostriction, as given by the Maxwell relation $\left(\frac{\partial V}{\partial H}\right)_{P,T} = -\left(\frac{\partial M}{\partial P}\right)_{H,T}$ [13].

The magnetic exchange couplings, J, have been reported in Fig. 4 and some important values are listed in Table 2. The largest couplings correspond to Co–Co and Co–Ni interactions, followed by Ni–Ni, which are an order of magnitude smaller. Interactions between Co and Ga are negligible and are not expected to affect the magnetic properties of the system in a noticeable manner. The calculated J have been found to be of the same order of magnitude as reported in the literature for other Heusler structures, e.g. for Fe_2CoGa, $J_1^{Fe–Fe} = 18$ meV and $J_2^{Fe–Fe} = 1$ meV [40]. The larger magnitude of the interactions in the Fe-based Heusler system can be attributed to the larger magnetic moment of Fe leading to strong Fe–Fe interactions. Our results also agree well with the experimental and calculated values of Co_2MnSi [47, 48]. The Curie temperature for Co_2MnSi has been found to be small, in accordance with our results, showing a similar dependence of the magnetic couplings. In general, the magnetic exchange couplings decay with distance. The Co–Co interaction decays slowly but vanishes after the fifth next neighbor. The fourth next nearest neighbors are weakly anti-ferromagnetic as compared to the neighboring shell interactions. In the case of Co–Ni, the decay is much faster than the Co–Co interaction but the magnetic coupling is almost as strong, at least for the closest neighbors. As mentioned earlier, the Ni–Ni interaction is an order of magnitude smaller than the Co–Co interaction. In this case, the nearest neighbor interactions are antiferromagnetic while other interactions are ferromagnetic in nature.

The nearest neighbor interaction parameter, for all the atoms, has been found to be always the strongest except Ni–Ni. and these interactions are comparable to some and smaller than other Co-based Heusler compounds [49]. In any case, the strength of the interaction depends on the magnitude of the local magnetic moment. The effect of pressure is most dominant on the nearest neighbor couplings. The variation of coupling parameters has been found to be uniform with respect to the pressure except for the Co–Co coupling, in which case the second nearest interaction parameters does not vary, while the first and third neighbor coupling parameters change non-uniformly (the ferromagnetic coupling changes from almost 2.0 meV to 1.0 meV up to 18 GPa, while the changes in the antiferromagnetic coupling is much smaller). Again, this drastic change in the strength of the ferromagnetic coupling in Co past 12 GPa can be related to the qualitative changes of the electronic DOS of the majority channel close to the Fermi level (see Fig. 2 and related discussion).

The calculated values of the total magnetic moment are small, so the Curie temperatures are also expected to be small compared with localized magnetic systems, in which T_C can be higher than 600 K. These results correlate well with the small electron localization described by LSDA calculations. The Curie temperature is large in case the localization is large and there is a good chance that LSDA may not be able to describe the strong correlation contributions correctly. Some specific values have been reported in Table 1 and the total pressure dependence can be observed in Fig. 5. One can observe an inflection in the pressure dependence of T_C starting at about 12 GPa. This rapid decrease in T_C is due to the weakening of the first and third Co–Co magnetic coupling parameters, which are also related to significant changes in the population majority channel at the Fermi level, as described above. Figure 5 shows the calculated mean-field Curie temperatures. These results are close to the ones reported for Co_2VGa and Co_2TiAl but much lower than Co_2MnGa, which is close to 700 K. The results of the Curie temperature from mean field approximation agree well with the results of the Monte Carlo simulations, which strengthen the reliability of the calculations. Ignoring the second-order features of the pressure dependence of T_C, one can analyze the overall change in T_C

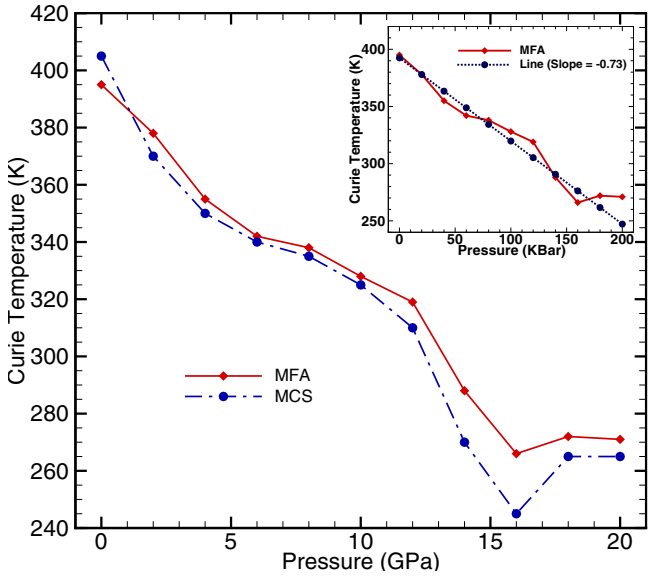

Figure 5 (online color at: www.ann-phys.org) Calculated Curie temperature of Co_2NiGa in a $L2_1$ crystalline structure under pressure.

as a function of pressure. Our analysis yields a pressure dependence of about $-0.73\ \frac{\mathrm{K}}{\mathrm{kbar}}$. As can be seen in Table 3, this value is consistent with experimental measurements of $\frac{dT_C}{dP}$ for different Co_2XY Heusler systems. The actual pressure dependence of T_C is ultimately controlled by the electronic properties of the materials, such as d-band widening and s-d charge transfer [50]. As we discussed above, higher pressure and shorter interatomic distances lead to increased overlap and decreased localization, resulting in smaller magnetization. The negative sign of $\frac{dT_C}{dP}$ is also consistent with weak itinerant ferromagnets [51]. Notice that $\frac{dT_C}{dP}$ has the same sign as $\frac{dM}{dP}$. According to the analysis by Takahashi and collaborators [52], the equality in sign of the pressure dependence of magnetization and Curie temperature is due to the significant variation of the magnetic moment with pressure.

The effect of pressure on the Curie temperature and (saturation) magnetization has been analyzed within the framework of Stoner-Edwards-Wohlfarth theory (SEW), where the free energy is expanded as function of the magnetization with parameters that depend on the volume change and the temperature [52]. This approach is valid for strong ferromagnets but not for weak itinerant ferromagnets [57]. According to SEW, $\frac{d\log M}{dP} = \frac{d\log T_c}{dP}$. For weak itinerant ferromagnets, on the other hand, spin fluctuations need to be considered in the magnetic free energy expansion and it shows a different dependence of

Table 3 Parameters typical weak itinerant electron ferromagnets.

Compounds	T_c(K)	dT_c/dP (K/kbar)	References
Co_2ZrAl	180	-0.40	T. Kanomata et al. [53]
Co_2TiAl	124.5	-0.70	E. DiMasi et al. [54]
Co_2TiGa	128	-1.27	T. Sasaki et al. [55]
Co_2VGa	357	-0.78	T. Kanomata et al. [56]
Co_2NiGa	395	-0.73	This work

the Curie temperature and magnetization with pressure. Such description has been discussed in the literature, for example in Refs. [52, 55, 57]. In the case of weakly itinerant magnetism, the relationship between the pressure dependence of the Curie temperature and the pressure dependence of magnetization is expected to be $\frac{d\log M}{dP} = \frac{2}{3}\frac{d\log T_c}{dP}$. Figure 6 shows a plot of $\ln(M)$ vs. $\ln(T_C)$. The slope of this plot (excluding the two points corresponding to the highest pressures considered, 18 and 20 GPa) is actually very close to $\frac{2}{3}$, indicating that the behavior of Co_2NiGa is that of a weakly itinerant ferromagnet. This point is strengthened if we also observe that the magnetic moment decreases with pressure as this is mainly

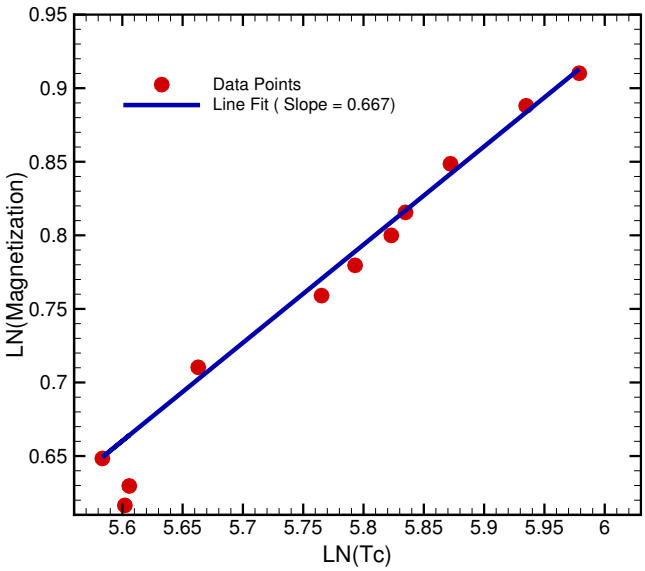

Figure 6 (online color at: www.ann-phys.org) Interdependence of Magnetization and Curie temperature for Co_2NiGa systems under increased pressures on a natural log–log scale. The slope of the line is approximately 2/3, an expected (theoretical) value for $\ln(M)$ vs. $\ln(T_C)$ curve for weak itinerant ferromagnets.

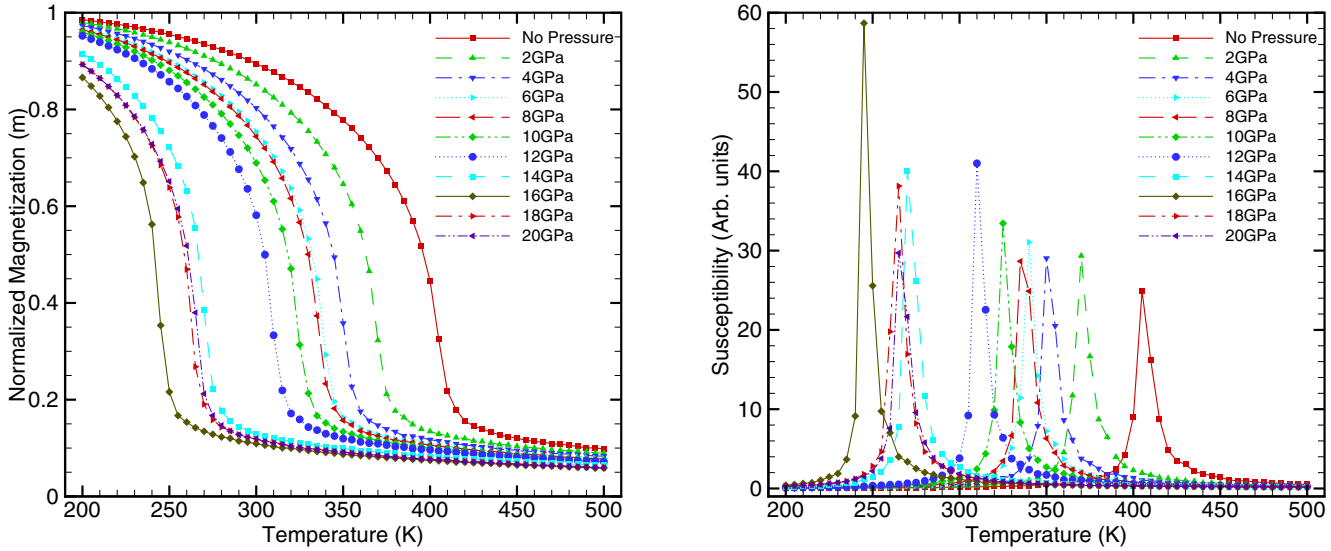

Figure 7 (online color at: www.ann-phys.org) Normalized magnetization and magnetic susceptibility as a function of temperature calculated using Monte Carlo simulations.

due to the itinerant nature of the d electrons in Co and Ni.

As mentioned above, we used Monte Carlo simulations to investigate the magnetic properties of Co_2NiGa as a function of temperature and pressure. These calculations take into consideration the magnetic exchange constants obtained using the SPRKKR method. As mentioned above, the calculated Curie temperatures using Monte Carlo simulations agreed rather well with the mean-field approximation, as shown in Fig. 5. The behavior of the (normalized) magnetization and magnetic susceptibility as a function of temperature and pressure is shown in Fig. 7. The figure shows that pressure has a significant effect on the temperature dependence of the magnetic properties of the system. The results indicate, for example, that as pressure increases, the paramagnetic state is stabilized with respect to the ferromagnetic phase, decreasing the Curie temperature of the system by more than 100 K over 18 GPa pressure change. The plot of the normalized magnetization also suggests a non-uniform change with pressure: after a rapid drop in T_C at low pressures, the rate of change of T_C with pressure is somewhat arrested, only to become even more pronounced after about 12 GPa. This seems to be correlated to the qualitative changes in the electronic density of the majority channel close to the Fermi level at around the same pressure. The plot of the temperature dependence of the magnetic susceptibility at different pressures shows similar trends. Closer inspection of Fig. 7 shows that the Monte Carlo simulations corresponding to 16 GPa actually fall outside the trend observed for the rest of the pressure conditions. This is also consistent with the calculated T_C in which a clear dip at 16 GPa can be observed. At this moment, it is not possible to determine the reason for this behavior although it is very likely due to the non-linear behavior of the electronic DOS at the Fermi level, although numerical issues related to the calculation of the magnetic couplings cannot be ruled out.

Figure 8 shows the structure factor dynamic $S(\mathbf{q},\omega)$ along the $\mathbf{q}$-value [100]. The observed excitations corresponding to the two modes or branches. The number of branches in the spectrum is equal to the number of magnetic atoms in the unit cell [58–60], therefore Co_2NiGa has two branches. One of the branches is acoustic and has zero energy for $\mathbf{q} = 0$, with a q^2 dependence for low q [60, 61]. In Co_2NiGa, the acoustic branch is predominantly of the Co type stemming from the weak interaction between Ni and Ga magnetic moments, a supported observation from the exchange magnetic couplings and the atomic magnetic moment (magnon energy is proportional to these two quantities). The acoustic spin wave mode remains practically undamped for spin-wave momenta in the entire Brillouin zone. On the contrary, the optical modes feature a finite life-time changing strongly and non-monotonously as function of the spin momentum [58]. The optical mode exist partially over the Brillouin zone along the [100] direction. This can be shown to be caused by the large density of Stoner (spin-flip) excitations which occur near the average spin-splitting energy near the Fermi surface. Those excitations are typi-

cal from weakly itinerant compounds. A prerequisite for spin-flip scattering is the availability of empty minority states at the Fermi level, which means a finite polarization. For this reason, a reduction in or lack of available minority phase space should therefore limit spin-flip events and slow down the demagnetization after an ultrafast excitation. Half-metals are a perfect system to test this hypothesis [62–65]. This behavior has also been reported for different materials studied such as Ni, Fe and Co [66–68].

The dispersion curve does follow a cosinusoid dependence with q with a maximum value at $q = 0.5$ for 0, 6 and 12 GPa (Fig. 8(a–c)). On the other hand, for the magnon calculations at 18 GPa, the acoustic dispersion follows an almost linear behavior but with small curvature around the maximum. After $q = 0.5$, there is the appearance of a second magnon branch which is less dispersive and appears up to values of $q = 0.8$. Even though, our calculations were unable to identify the uniqueness of this branch, the decay of the acoustic magnon after $q = 0.5$ occurs in the same interval of q [0, 0.5]. The complexity of the magnon dispersion relation is not smooth, meaning that it requires several Fourier components to describe the intimate details.

Table 4 Maximum value of the dynamical structure factor at $q = 0.5$ along the [100] direction in the Co_2GaNi system.

GPa	acoustic (meV)	optic (meV)	difference)
			acoustic-opt. (meV)
0	139.672	205.632	65.672
6	118.474	194.060	75.586
12	122.314	184.802	62.488
18	118.686	161.659	42.686

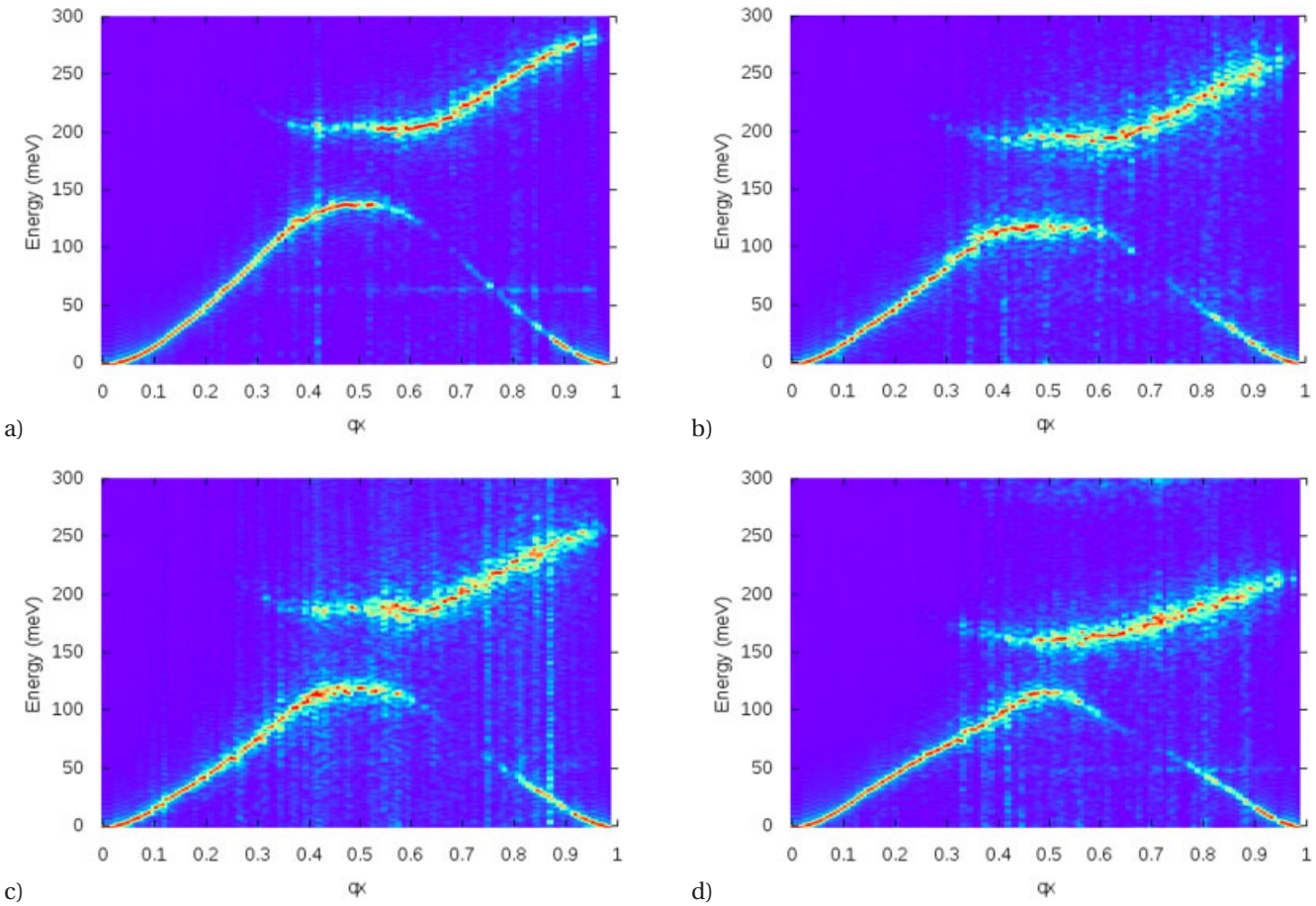

Figure 8 (online color at: www.ann-phys.org) Dynamic structure factor, $s(\mathbf{q}, \omega)$ of Co_2GaNi along the [100] direction for a) 0.0 GPa b) 6.0 GPa c) 12.0 GPa d) 18 GPa.

After the pressure is applied, the behavior around the maximum value of $q = 0.5$ is smooth and as the pressure increases the trends are clearer. The second branch is increasing its intensity and at pressures of 18 GPa, it appears as a non dispersive energy relation. It is expected that the change of the exchange magnetic couplings should play a very important role and we will explore this possibility in the near future.

In order to compare the pressure changes induced in the dynamical structure factor, we report in Table 4 the energy values at the maximum, which corresponds to q values close to 0.5. At it can be seen, pressure induces an increase in the magnon energy and changes in the position of the optical branch, which was observed when q changes from $[0.5, 1.0]$.

5 Conclusion

Herewith we report a theoretical study of the structural, magnetic and spin dynamics of the Heusler alloy Co_2NiGa with the $L2_1$ crystal structure under pressure. We find agreement of all structural and elastic properties with reported experimental and/or theoretical values. The compressibility dependence of the volume is quadratic with the pressure and the coefficients were determined. Based on the obtained equation of states, we are able to study the changes of the magnetic properties as function of pressure.

The electronic DOS at the Fermi level is dominated by d-states, which in turn are contributed mostly by the cobalt atoms. An analysis of the relative changes in the populations of majority and minority states at the Fermi level shows that Co_2NiGa is not really a half-metal, although the population of states of the majority channel is significantly lower than that of the majority channel, yielding a polarization of the order of -0.52 at the ground state. As pressure increases, there is an overall increase of the polarization to about -0.57 at 18 GPa. Inflections in the overall trend in the pressure dependence of the polarization at pressures close to 12 GPa seem to be correlated to qualitative changes in the electronic DOS of the majority channel at the Fermi level.

As pressure is increased, interatomic distances shorten. This is accompanied by depletion of the d-band, increased overlapping of d-states and an increased metallicity and delocalization. This result in a decrease in magnetization with pressure, with changes of about 15% over 20 GPa. This negative pressure dependence of the magnetization leads to a positive value for the isotropic magnetostriction. The calculated magnetic exchange couplings are mostly dominated by Co–Co and Co–Ni interactions. Our calculations show them to be affected by pressure, with the Co–Co couplings changing the most. Close examination of the pressure dependence of the Co–Co magnetic couplings suggests that the change is not uniform across the different nearest neighbor interactions.

The Curie temperatures calculated using the mean-field approximation and Monte Carlo simulations doe not have a simple dependence with pressure but in general, there is a monotonic decrease as function of pressure. The negative pressure dependence (-0.73 K/Kbar) of T_C compares well with experimental measurements in other Co_2XY systems. The pressure dependence of the Curie temperature and the total magnetization reveals the weakly itinerant magnetism of this compound, where a model incorporating spin fluctuations yields the relationship $\frac{d\log M}{dP} = \frac{2}{3}\frac{d\log T_c}{dP}$. This relationship seems to hold even at the highest pressures studied.

The dynamical structural factor was also calculated, which represents the magnon spectra. We are able to reproduce the cosinusoidal behavior at low pressures but as the pressure is increased a large linear dispersion was found. An optical branch was observed, which does not extend over the whole Brillouin zone and which is consistent with local spin flips and consistent with weak itinerant ferromagnets as it is also determined by relating the changes in the Curie temperature with the crystal magnetization. The optical-acoustic gap decreases slowly as function of pressure. Explorations with temperature and along other crystallographic directions are on their way.

Acknowledgements. We would like to thank Prof. Ulrich Eckern for all these years of great collaboration and discussions, your friendship is quite valuable. We (A. H. R, E. O., A. L. M.) acknowledge support from CONACYT-México under projects 152153 and PPPROALMEX-DAAD-CONACYT. R. A. would like to acknowledge the National Science Foundation (Grants No. DMR-0844082 and DMR-0805293) for partial support to complete this work. We also recognize the support by TAMU-CONACYT bi-national collaboration. Some first-principles calculations were carried out in the Chemical Engineering cluster of Texas A&M University, the Texas A&M Supercomputing Facility, the CNS-IPICyT, Mexico and the Ranger cluster at the Texas Advanced Computing Center (TACC) at the University of Texas in Austin.

Key words. Spin dynamics, heusler alloys, magnetic exchange couplings, magnetic systems under pressure.

References

[1] C. Felser, G. H. Fecher, and B. Balke, Angew. Chem. Int. Ed. **46**(5), 668–699 (2007).
[2] S. Kämmerer, A. Thomas, A. Hütten, and G. Reiss, Appl. Phys. Lett. **85**, 79–81 (2004).
[3] K. Ozdogan, E. Sasioglu, and I. Galanakis, arXiv:0801.2252 (2008).
[4] I. Žutić, J. Fabian, and S. Das Sarma, Rev. Mod. Phys. **76**, 323–410 (2004).
[5] P. Entel and V. D. Buchelnikov, J. Phys. D: Appl. Phys. **39**(5), 865 (2006).
[6] D. Wagner and E. Wohlfarth, J. Phys. F: Metal Phys. **11**, 2417 (1981).
[7] N. Lanska and K. Ullakko, J. Appl. Phys. Lett. **80**, 1746 (2002).
[8] M. Zhang, E. Bruck, F. R. de Boer, and W. Guangheng, J. Phys. D: Appl. Phys. **38**(9), 1361 (2005).
[9] M. Siewert, M. E. Gruner, and Dannenberg, Phys. Rev. B **82**, 064420 (2010).
[10] P. J. Brown et al., J. Phys.: Condens. Matter **17**(8), 1301 (2005).
[11] X. Dai et al., J. Appl. Phys. **101**(9), 09N503 (2007).
[12] R. Arróyave, A. Junkaew et al., Acta Mater. **58**(16), 5220–5231 (2010).
[13] D. Gugan, Proc. Phys. Soc. **72**, 1013 (1958).
[14] G. Kresse and J. Furthmüller, Phys. Rev. B **54**, 11169–11186 (1996).
[15] G. Kresse and D. Joubert, Phys. Rev. B **59**, 1758–1775 (1999).
[16] H. Ebert, The Munich SPR-KKR package Version 5.4 (2005).
[17] H. Ebert, J. Minar, and V. Popescu,Lecture Notes in Physics **580**, 371 (2001).
[18] J. Minar, A. Perlov, H. Ebert, and H. Hashizume, J. Phys.: Condens. Matter **17**, 5785 (2005).
[19] A. Liechtenstein, M. Katsnelson, V. Antropov, and V. Gubanov, J. Magn. Magn. Mater. **67**(1), 65–74 (1987).
[20] E. Şaşıoğlu, L. Sandratskii, and P. Bruno, Phys. Rev. B **70**, 024427 (2004).
[21] M. Meinert, J. Schmalhorst, and G. Reiss, J Phys.: Condens. Matter **23**, 036001 (2011).
[22] L. Landau and E. Lifshitz, Phys. Z. Sowjetunion **8**(14), 14–22 (1935).
[23] L. Gilbert, Trans. Magn. **40**(6), 3443 (2004).
[24] B. Skubic, J. Hellsvik, L. Nordstrom, and O. Eriksson, J. Phys.: Conden. Matter. **20**(31), 315203 (2008).
[25] J. Hellsvik and Skubic, Phys. Rev. B **78**(10), 144419 (2008).
[26] V. Kamberský, Czech. J. Phys. **26**, 1366–1383 (1976).
[27] M. Oogane et al., Jpn. J. Appl. Phys. **45**(5A), 3889–3891 (2006).
[28] K. Gilmore, Y. U. Idzerda, and M. D. Stiles, Phys. Rev. Lett. **99**, 027204 (2007).
[29] J. P. Perdew, K. Burke, and M. Ernzerhof, Phys. Rev. Lett. **77**, 3865–3868 (1996).
[30] S. Trudel et al. J. Phys. D: Appl. Phys. **43**(19), 193001 (2010).
[31] H. C. Kandpal, G. H. Fecher, and C. Felser, J. Phys. D: Appl. Phys. **40**(6), 1507 (2007).
[32] S. Mizukami et al., J. Appl. Phys. **105**(7), 07D306 (2009).
[33] R. Yilgin et al., Jpn. J. Appl. Phys. **46**(9), L205–L208 (2007).
[34] I. Galanakis, Phys. Rev. B **71**, 012413 (2005).
[35] V. Buchelnikov et al., Phys. Rev. B **81**(9), 094411 (2010).
[36] T. Castán, E. Vives, and P. Lindgård, Phys. Rev. B **60**(10), 7071 (1999).
[37] N. Singh, E. Dogan, I. Karaman, and R. Arróyave, Phys. Rev. B **84**(18), 184201 (2011).
[38] A. Ayuela, J. Enkovaara, K. Ullakko, and R. Nieminen, J. Phys: Condens. Matter **11**, 2017 (1999).
[39] J. Bai et al., Solid State Phenom. **160**, 69–74 (2010).
[40] A. Dannenberg, M. Gruner, M. Wuttig, and P. Entel, Characterization of New Ferromagnetic Fe-Co-Zn-Ga Alloys by ab initio Investigations, in: ESOMAT 2009 – 8th European Symposium on Martensitic Transformations (2009), p. 4004.
[41] A. G. Gavriliuk, G. N. Stepanov, V. A. Sidorov, and S. M. Irkae, J. Appl. Phys. **79**, 2609 (1995).
[42] J. De Teresa et al., Appl. Phys. Lett. **82**(21), 4288–4291 (1999).
[43] E. Şaşıoğlu, L. Sandratskii, and P. Bruno, Phys. Rev. B **71**(21), 214412 (2005).
[44] J. Bai, J. Appl. Phys. **109**, 014908 (2011).
[45] A. Carbonari et al., J. Magn. Magn. Mater. **163**(3), 313–321 (1996).
[46] I. Galanakis and P. H. Dederichs, Phys. Rev. B **66**, 174429 (2002).
[47] E. Şaşıoğlu, L. Sandratskii, P. Bruno, and I. Galanakis, Phys. Rev. B **72**(18), 184415 (2005).
[48] Y. Kurtulus, R. Dronskowski, G. Samolyuk, and V. Antropov, Phys. Rev. B **71**(1), 014425 (2005).
[49] J. Kübler, G. Fecher, and C. Felser, Phys. Rev. B **76**(2), 024414 (2007).
[50] H. Fujiwara, H. Kadomatsu, K. Ohishi, and Y. Yamamoto, J. Phys. Soc. Jpn. **40**(4), 1010–1016 (1976).
[51] M. Shimizu, J. Magn. Magn. Mater. **20**(1), 47–55 (1980).
[52] Y. Takahashi and H. Nakano, J. Phys.: Condens. Matter **18**, 521 (2006).
[53] T. Kanomata et al., Phy. Rev. B. **82**(14), 144415 (2010).
[54] E. DiMasi, M. Aronson, and B. Coles, Phy. Rev. B **47**(21), 14301 (1993).
[55] T. Sasaki et al., J. Alloys Compd. **317–318**, 406–410 (2001).
[56] T. Kanomata, J. Alloys Compd. **393**(1–2), 26–33 (2005).
[57] Y. Takahashi,J. Phys.: Condens. Matter **6**, 7063 (1994).
[58] P. Buczek, A. Ernst, P. Bruno, and L. M. Sandratskii, Phys. Rev. Lett. **102**, 247206 (2009).
[59] H. C. Kandpal, G. H. Fecher, and C. Felser, J. Phys. D: Appl. Phys. **40**(6), 1507 (2007).

[60] K. Tajima et al., J. Phys. Soc. Jpn. **43**(2), 483–489 (1977).
[61] Y. Noda and Y. Ishikawa, AIP Conf. Proc. **40**(3), 699–704 (1976).
[62] P. Mavropoulos, I. Galanakis, V. Popescu, and P. Dederichs, J. Phys.: Condens. Matter **16**, S5759 (2004).
[63] L. Chioncel, E. Arrigoni, M. Katsnelson, and A. Lichtenstein, Phys. Rev. Lett. **96**(13), 137203 (2006).
[64] D. Edwards and J. Hertz, J. Phys. F: Metal Phys. **3**, 2191 (1973).
[65] G. Müller et al., Nature Materials **8**(1), 56–61 (2008).
[66] R. Świrkowicz, Physica B: Condens. Matter **160**, 329–337 (1990).
[67] H. A. Mook and D. M. Paul, Phys. Rev. Lett. **54**, 227–229 (1985).
[68] M. Pajda, Phys. Rev. B **64**, 174402 (2001).